Development of a discharge-free pre-treatment device for spent lithium-ion batteries under an inert atmosphere

Sung-Hoon Jung[1], Jong-Min Jung[2], Jei-Pil Wang[1*]

[1]Department of Metallurgical Engineering, Pukyong National University, Busan 48513, Korea.
[2]Department of Energy Industrial Equipment, Ulsan Campus of KOREA POLYTECHNIC, Ulsan 44482, Korea.

Corresponding author: Jei-Pil Wang (*Email: jpwang@pknu.ac.kr*)

Abstract

This study designs, fabricates, and experimentally validates an inert-atmosphere, discharge-free pre-treatment device for spent lithium-ion batteries (LIBs). The system integrates a vacuum pass-box with a processing enclosure (shredder and drying furnace) and enables continuous comminution and thermal drying while maintaining an internal oxygen concentration of $\leq 3\%$ under argon. Trials on cylindrical 18650 cells involved vacuum loading, shredding, and a 300 °C, 2 h thermal step. Mass balance indicated an electrolyte-removal fraction of 5.3%, and the recovered black powder exhibited preserved NCM-type cathode signatures together with Cu/Al from current collectors, as confirmed by XRD, XRF, and SEM-EDS. Potentially harmful HF/HCl off-gases were neutralized in a NaOH scrubber prior to discharge. Compared with conventional brine-discharge → shredding → drying workflows, the proposed device mitigates wastewater and odor, suppresses ignition risk through atmosphere control, and is amenable to continuous, automation-ready operation, providing a practical alternative for industrial LIB recycling lines.

Keywords: Electrolyte removal, Inert atmosphere, Lithium-ion battery, Pre-treatment, Shredding, Spent LIB recycling.

Competing Interests: The authors declare that they have no competing interests.
Authors' Contributions: All authors contributed equally to the conception and design of the study. All authors have read and agreed to the published version of the manuscript.
Transparency: The authors confirm that the manuscript is an honest, accurate, and transparent account of the study; that no vital features of the study have been omitted; and that any discrepancies from the study as planned have been explained. This study followed all ethical practices during writing.

1. Introduction

Driven by global efforts toward climate mitigation and carbon neutrality, demand for electric vehicles (EVs), stationary energy-storage systems (ESS), and portable electronics has surged, accelerating the deployment of lithium-ion batteries (LIBs) as the dominant energy-storage technology. Market analyses project a compound annual growth rate

exceeding 10.3% through 2033, and with major automakers announcing plans to phase out internal-combustion vehicles by 2040, LIB use in transportation is expected to expand further [1-4]. Consequently, the volume of spent lithium-ion batteries (spent LIBs) will rise sharply. Beyond the value of recoverable metals (Cu, Ni, Co, Li), spent LIBs contain residual electrolyte and stored electrical energy, both of which pose significant hazards—short circuits, thermal runaway, fire, and explosion—if not handled properly. Safe and environmentally responsible pre-treatment is therefore essential, not merely resource recovery [5].

Conventional pre-treatment flows for spent LIBs typically involve three sequential steps: (i) salt-solution discharge, (ii) mechanical dismantling/shredding, and (iii) thermal drying/electrolyte removal. Each step carries technical and environmental drawbacks [6, 7]. First, brine discharge can generate odorous wastewater containing organic solvents and heavy-metal species, imposing high treatment costs and increasing the risk of regulatory non-compliance as environmental standards tighten [8]. Second, incomplete discharge leaves residual energy that can cause shorting during shredding, leading to spark, fire, or explosion—threatening worker safety and undermining process reliability [9]. Third, most commercial shredders operate in single-batch mode and struggle to maintain an inert atmosphere continuously, resulting in frequent stops, operator intervention, limited scalability, and weak coupling to automation [10].

To address these technical, environmental, and economic limitations, this work develops a pre-treatment system that eliminates brine discharge yet enables safe shredding and electrolyte removal. The system is built around a dual-chamber architecture—a pass-box for continuous feed and a processing module—capable of establishing vacuum and inert atmospheres simultaneously. It is designed for continuous input and automated control, allowing uninterrupted pre-treatment of spent LIBs. Critically, the internal oxygen concentration is maintained at $\leq 3\%$, suppressing combustion risk during size reduction. Harmful off-gases generated during thermal treatment of the electrolyte (e.g., HF, HCl) are routed to a scrubber, where pH is neutralized prior to emission. In doing so, the proposed system overcomes structural limitations of legacy pre-treatment lines and provides a process model suitable for industrial scale-up and automation-ready deployment.

2. System Fabrication
2.1. Enabling technology and design rationale

Conventional pre-treatment of spent lithium-ion batteries (LIBs) typically relies on brine discharge followed by mechanical size reduction, thermal drying for electrolyte removal, and classification to obtain a recyclable black-powder product. When cells are not fully discharged, however, residual energy can precipitate shorting during comminution and lead to sparks, fire, or even explosions. Although brine discharge and subsequent drying mitigate that risk, they generate odorous, metal-bearing wastewater and extend overall cycle time, thereby burdening both environmental compliance and throughput.

The apparatus developed in this study removes the brine-discharge step while preserving process safety by maintaining inert conditions throughout all unit operations. As depicted schematically in Figure 1, the system consists of two coupled volumes: a pass-box dedicated to continuous feeding and a processing chamber in which shredding and thermal electrolyte removal are executed. Spent LIBs first enter the pass-box, where the headspace is evacuated by a vacuum pump and then backfilled with high-purity argon (Ar), establishing an oxygen-free atmosphere. In parallel, the processing chamber is continuously purged with Ar so that the internal oxygen concentration remains below 3%, a threshold selected to suppress combustion during mechanical breakage and hot operations. Transfer between the two spaces occurs only after their atmospheres are matched; an interlock mechanism permits passage from the pass-box into the processing chamber without breaking inert conditions. In this way, continuous feeding is achieved while the entire line remains isolated from ambient air. Within the processing chamber, batteries are reduced in size and subsequently dried to remove residual electrolyte under the same Ar-rich environment. Off-gases evolved during heating—including HF and HCl—are routed to a downstream gas-handling train composed of a heated dryer and a wet scrubber. There, the stream is neutralized under pH control prior to discharge, addressing the environmental liabilities intrinsic to brine-based discharge and conventional drying steps. By combining vacuum conditioning in the pass-box with low-oxygen Ar purging in the processing chamber, the apparatus enables continuous, automation-ready pre-treatment with reduced ignition risk, no aqueous discharge, and an integrated exhaust system that neutralizes acid gases before release.
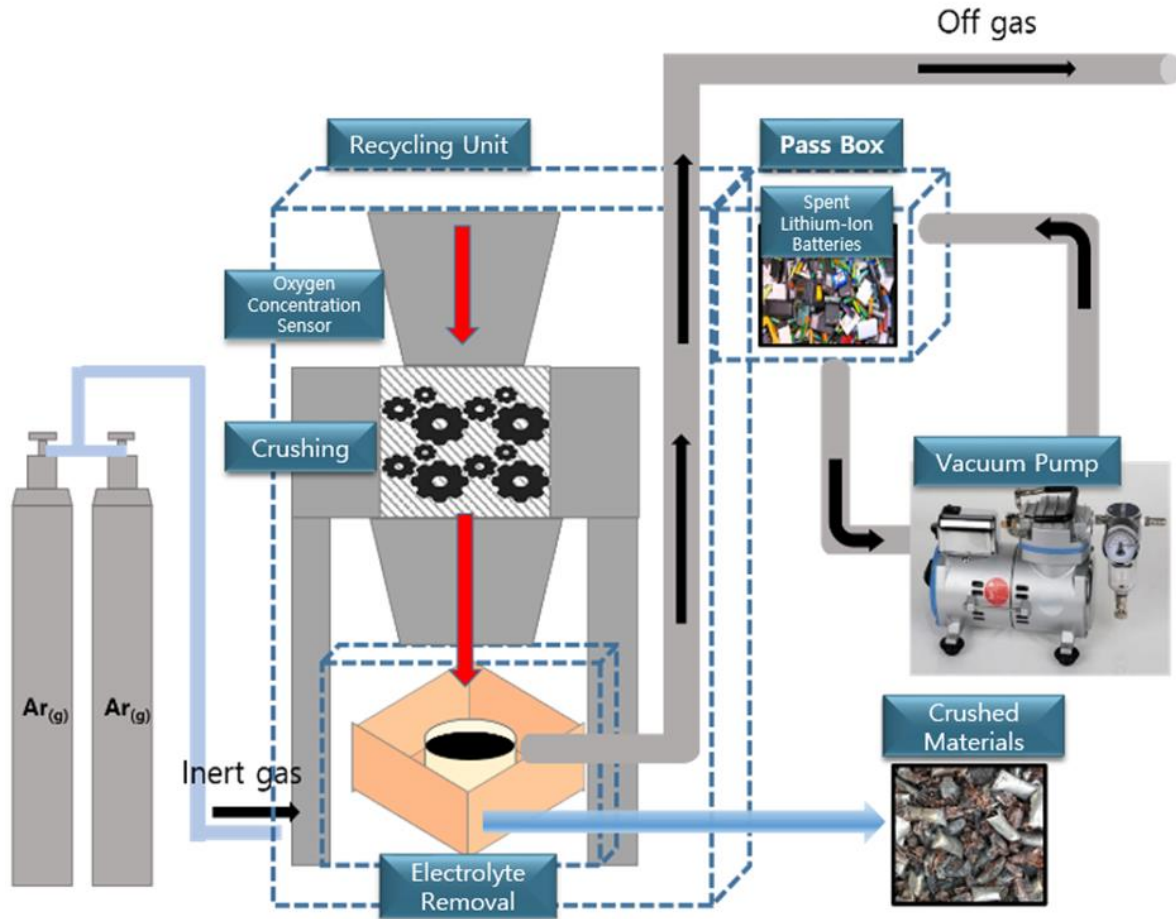
Figure 1.
Schematic of the pre-treatment apparatus.

2.2. Equipment configuration

As shown in Figure 2, the prototype comprises two primary volumes—a recycling (processing) section and a pass-box—with the processing section further divided into a shredder bay and a drying furnace bay. The two volumes are coupled through an interlocked transfer port so that materials can be moved without breaking the inert atmosphere.

Figure 2.
Front elevation of the shredding/pre-treatment system.

2.2.1. Shredder

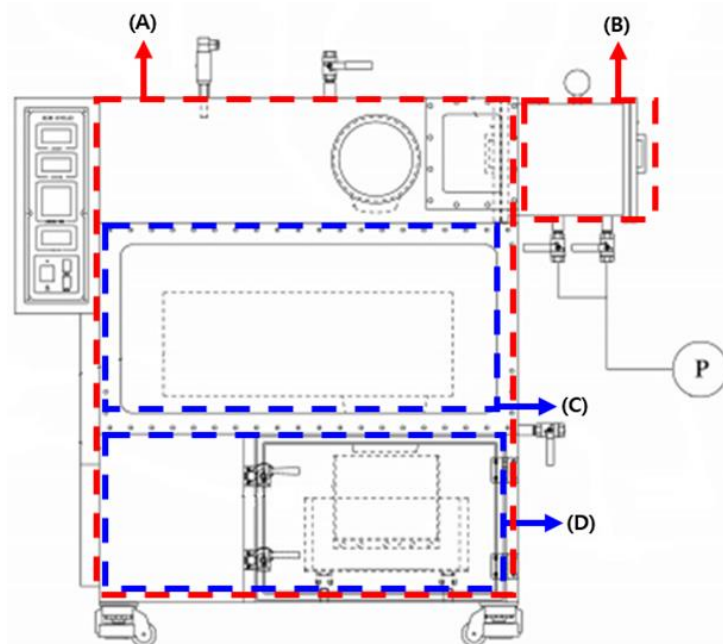The shredder mechanically breaks down spent lithium-ion batteries so that electrodes, separators, and current collectors can be physically liberated prior to downstream classification. As shown in Figure 3, the unit integrates what is typically implemented as a two– to three-stage reduction train into a single compact assembly, allowing continuous feed and stable processing of cells and modules with diverse form factors. The cutter box (feed opening $\approx 37 \times 27$ cm) houses counter-rotating, intermeshing cutter stacks that operate at low speed and high torque to minimize spark generation while producing a chip/flake mixture in which active material readily detaches from metallic foils. The gearbox-coupled drive and rigid frame are sized to provide the required torque margin for partially discharged packs while controlling vibration under inert atmosphere.

Figure 3.
Integrated low-speed/high-torque shredder for spent lithium-ion batteries.

2.2.2. Drying Furnace

The drying furnace removes electrolyte and residual moisture from the shredded battery fractions by controlled thermal treatment. As illustrated in Figure 4(A), the unit is installed directly beneath the shredder in a vertical, in-line configuration so that comminuted material is transferred by gravity without exposing the stream to ambient air. Inside the sealed furnace chamber, the atmosphere is maintained inert (Ar purge; $O_2 \leq 3\%$) and the load is heated to 300 °C for a prescribed dwell time, sufficient to volatilize carbonate-based solvents and entrained water and thus stabilize the resulting black powder for downstream handling. The chamber incorporates uniform heating elements and an exhaust takeoff connected to the facility's gas-handling train (dryer + wet scrubber), which neutralizes acid gases (e.g., HF, HCl) evolved during solvent removal. Interlocks prevent furnace access while at temperature or when the chamber atmosphere is not within the specified oxygen limit. This arrangement enables continuous, enclosed transfer from shredding to drying, minimizes ignition risk, and yields a dry, free-flowing product suitable for subsequent separation and metal recovery.
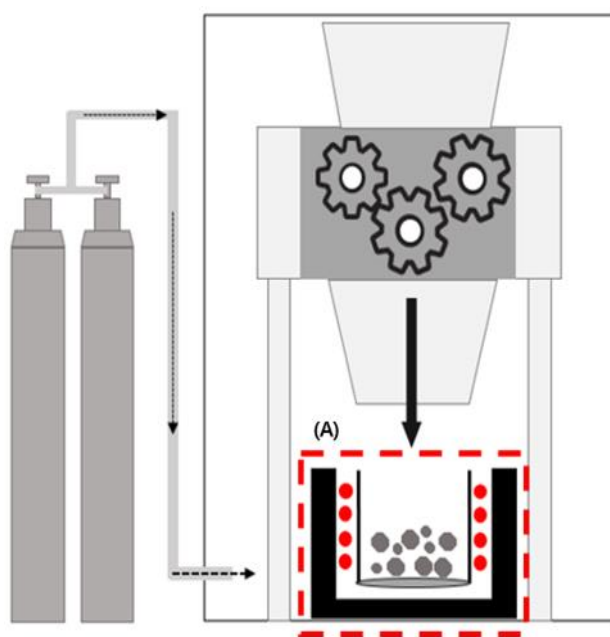

Figure 4.
Schematic of the drying furnace (A).
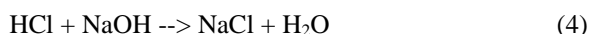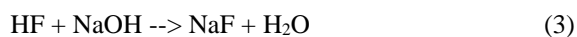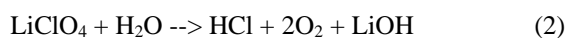
2.2.3. Gas-Injection Subsystem

The gas-injection assembly establishes and maintains the inert atmosphere required for safe operation. As shown in Figure 5, high-purity argon (Ar) is metered through a regulator and mass-flow control stage and introduced at the bottom of the processing enclosure, promoting upward displacement of residual air and uniform diffusion of the inert gas across the working volume. A distribution manifold with ball valves and check valves prevents backflow and allows section-by-section isolation during maintenance. The control objective is to keep the internal oxygen concentration at $\leq 3\%$; therefore, the Ar feed rate is closed-loop adjusted from an in-situ oxygen sensor signal, with fast purge "boost" and low-flow "hold" modes to minimize gas consumption while preserving the setpoint. Pressure is maintained slightly positive relative to ambient to suppress ingress at seals and transfer ports. This configuration provides stable, low-oxygen conditions throughout shredding and drying without interrupting continuous operation.

Figure 5.
Argon (Ar) injection hardware: (A) supply and flow-control panel; (B) bottom-entry injection line to the processing section for uniform inerting under O_2-sensor feedback control.

2.2.4. Gas Exhaust and Scrubbing System

The gas-exhaust subsystem safely removes volatile species generated during electrolyte evaporation and thermal treatment. Typical LIB electrolytes dissolve lithium salts such as $LiPF_6$, $LiClO_4$, or $LiBF_4$ in organic carbonate solvents (e.g., EC, PC, DEC, DMC) with small amounts of functional additives. During pre-treatment, these solvents volatilize or decompose; in particular, $LiPF_6$ can hydrolyze in the presence of moisture to produce HF and related acidic species, while $LiClO_4$ may likewise yield HCl under reactive conditions. Because HF and HCl are harmful to personnel and air quality, the exhaust stream is routed through a wet scrubber train prior to discharge (Figure 6). s implemented, the exhaust line (Figure 6A) draws from the sealed processing enclosure and delivers the flow to serial scrubber vessels (Figure 6B) charged with NaOH solution and a bromothymol blue (BTB) indicator for visual pH monitoring. Acid gases are neutralized according to the following representative reactions:

$$LiPF_6 + H_2O \rightarrow HF + PF_5 + LiOH \qquad (1)$$

$$LiClO_4 + H_2O \rightarrow HCl + 2O_2 + LiOH \qquad (2)$$

$$HF + NaOH \rightarrow NaF + H_2O \qquad (3)$$

$$HCl + NaOH \rightarrow NaCl + H_2O \qquad (4)$$

The system is operated to maintain near-neutral effluent pH at the scrubber outlet; BTB provides a rapid visual cue, and periodic grab samples confirm compliance. Flow is regulated to keep a slight negative pressure in the furnace/exhaust plenum, preventing fugitive emissions at seals while avoiding excessive solvent entrainment. In combination with the argon-purged, low-oxygen process atmosphere, this exhaust-and-scrubber arrangement enables continuous operation with controlled emissions and mitigated occupational exposure.

Figure 6.
Gas exhaust assembly: (A) exhaust takeoff from the processing enclosure; (B) two-stage NaOH/BTB
wet scrubber for neutralization and visual pH tracking prior to discharge.

2.2.5. Oxygen Sensor

An in-situ oxygen sensor continuously monitors the atmosphere inside the processing section to ensure safe operation during shredding and electrolyte drying. The control objective is to maintain $O_2 \leq 3\%$ at all times. The sensor output is fed to the gas-injection controller (Section 2.2.3), which adjusts argon flow between purge and hold modes to correct any excursions and minimize gas consumption. Alarm thresholds are implemented for both concentration and rate-of-rise; if either limit is exceeded, material transfer is inhibited and the interlock remains closed until the setpoint is restored. Periodic calibration against certified span gases is performed to ensure measurement fidelity over extended runs.

2.2.6. Inlet Cover

As shown in Figure 7, the inlet cover is a hinged, externally mounted door on the pass-box through which operators load spent LIBs. After loading, the door is closed to create a sealed vestibule isolated from ambient air, forming the basis for the subsequent evacuation–backfill sequence that establishes an oxygen-free condition prior to transfer. The cover employs a metal seat with a compressible gasket and toggle clamps to achieve repeatable sealing; a viewing port allows confirmation of payload position without opening the enclosure. Only when the pass-box atmosphere is matched to the processing section setpoint does the interlock open, ensuring that downstream operations remain in an inert environment.
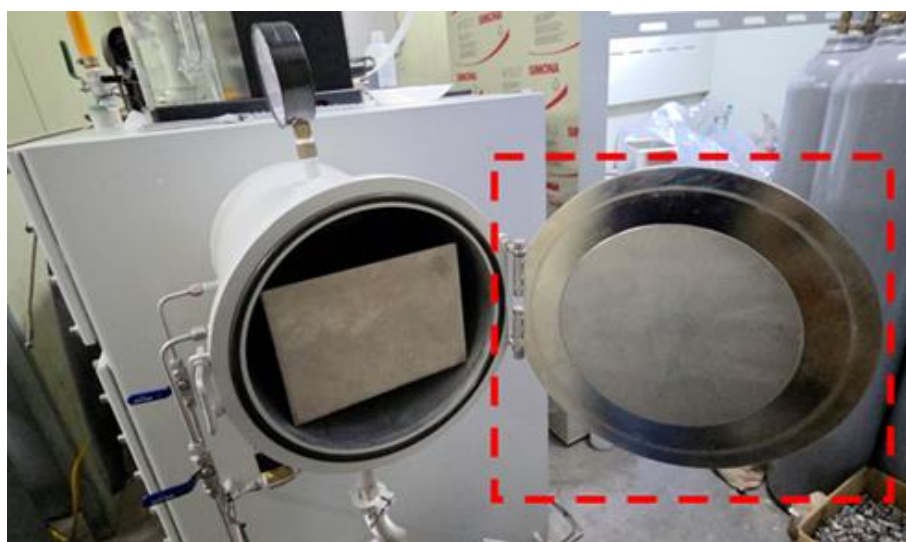
Figure 7.
Pass-box inlet cover (loading hatch) used to load spent LIBs while maintaining enclosure sealing.

2.2.7. Vacuum-Generation Unit

The vacuum-generation unit creates a low-pressure environment inside the pass-box and then backfills it with argon (Ar) so that its atmosphere matches that of the processing section. As shown in Figure 8, the assembly consists of a high-capacity vacuum pump (A) and an argon injection line within the pass-box (B). After loading spent LIBs, the pass-box headspace is evacuated to remove ambient air—thereby blocking the transfer of oxygen and moisture into the processing

enclosure—and simultaneously desorbing trace moisture from the battery surfaces. The chamber is subsequently backfilled with high-purity Ar and, if necessary, cycled through additional evacuate/backfill steps to reach the specified oxygen limit ($\leq 3\%$). This sequence enhances pre-treatment safety by preventing ingress of reactive species while preparing the payload for transfer under inert conditions.
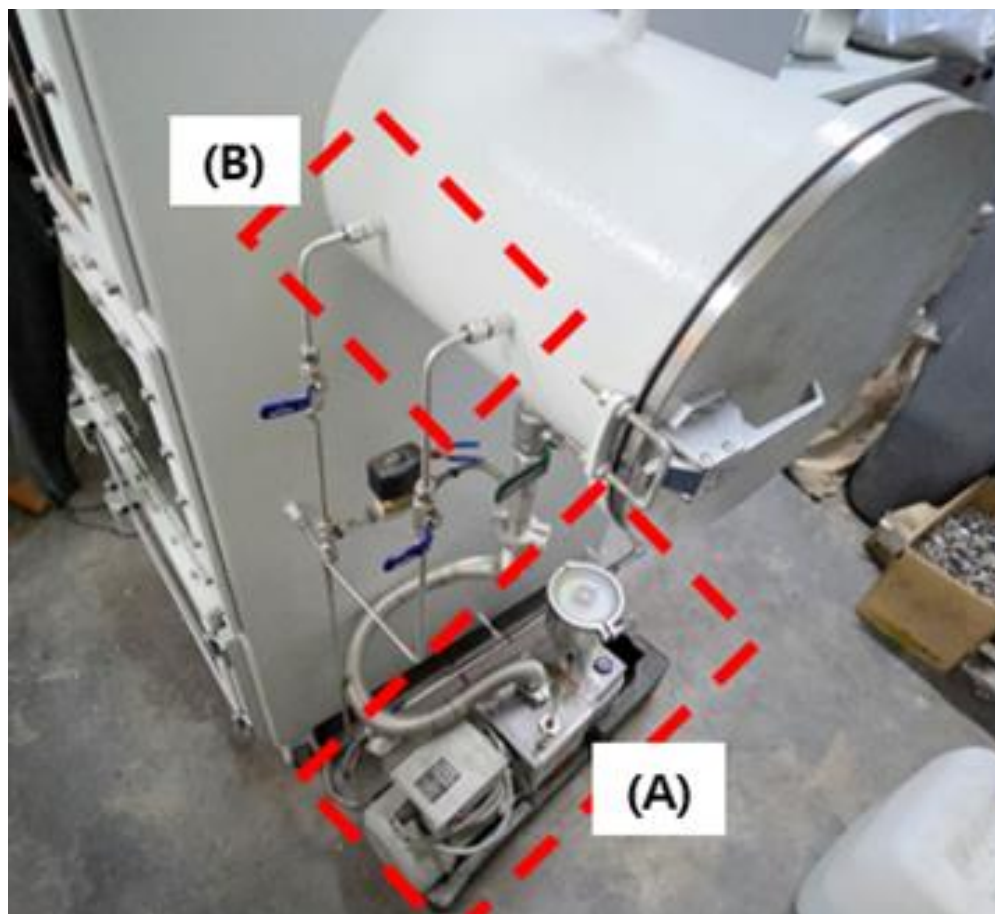

Figure 8.
Vacuum-generation unit for the pass-box: (A) high-capacity vacuum pump; (B) argon injection line used to backfill the evacuated vestibule and match the inert atmosphere of the processing section.

2.3. Experimental Procedure and Process Flow

Performance of the developed pre-treatment apparatus for spent LIBs was verified following the process flow shown in Figure 9. Prior to any material handling, the wet-scrubber train was charged with NaOH solution and a BTB indicator to neutralize acidic exhaust and to provide visual pH monitoring. The processing enclosure was then purged with high-purity argon until the in-situ O_2 sensor indicated an internal oxygen concentration of $\leq 3\%$, which was maintained throughout the run.
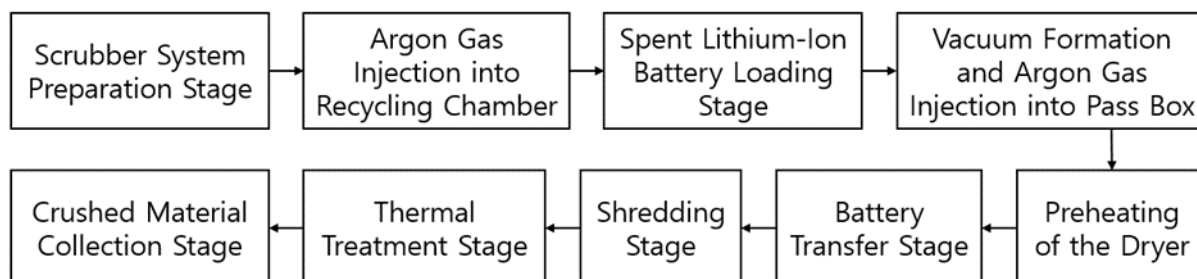
Figure 9.
Process flow for apparatus verification. From left to right.

Spent LIBs were loaded into the pass-box through the inlet cover and the vestibule was sealed. The headspace was evacuated with the vacuum pump and subsequently backfilled with argon to establish an oxygen-free atmosphere equivalent to that of the processing section; additional evacuate/backfill cycles were performed as needed to reach the O_2 set point while also desorbing trace surface moisture from the batteries.

In parallel, the drying furnace was preheated and stabilized at 300 °C. Once the atmospheres of the pass-box and processing section were matched, the interlock was opened and the batteries were transferred into the shredder bay.

Mechanical comminution proceeded under inert conditions, producing a fragmented mixture that fell by gravity directly into the Ar-purged furnace located beneath the cutter box. The load then underwent a 2-hour thermal soak at 300 °C, sufficient to volatilize electrolyte solvents and remove residual moisture.

After drying, furnace power was turned off and the chamber was allowed to cool below the defined safety threshold. The dried product (black powder and liberated foils) was recovered and collected for downstream handling. Throughout the procedure, oxygen concentration was monitored in real time to confirm atmosphere stability, and the exhaust stream was continuously routed through the NaOH/BTB scrubber to neutralize HF/HCl before discharge. The sequence was designed to evaluate, in a single integrated run, (i) environmental stability and inert-atmosphere control, (ii) shredding efficacy, and (iii) electrolyte-removal performance under continuous, automation-ready operation.

3. Results and Discussion

Using the inert-atmosphere pre-treatment apparatus, we evaluated both mechanical shredding and thermal electrolyte removal for spent LIBs under continuous operation. Results were benchmarked against conventional flows and analyzed quantitatively with emphasis on atmosphere stability, incident-free operation, and process continuity.

3.1. Process Safety Verified by Oxygen-Concentration Control

A key performance requirement is maintaining the oxygen level below 3% throughout shredding and drying to suppress ignition. During trials, the system remained stable with no signs of sparking, venting, or combustion, confirming effective control of the internal atmosphere by the bottom-entry Ar purge and sensor-feedback loop. As illustrated in Fig. 10, the measured oxygen concentration decreased from an ambient value of 21.0% O_2 to ≈ 2.3% O_2, and was held at this level during continuous operation. The result demonstrates that the gas-injection subsystem and in-situ O_2 sensor achieve the specified set point with sufficient margin, enabling safe, uninterrupted pre-treatment.
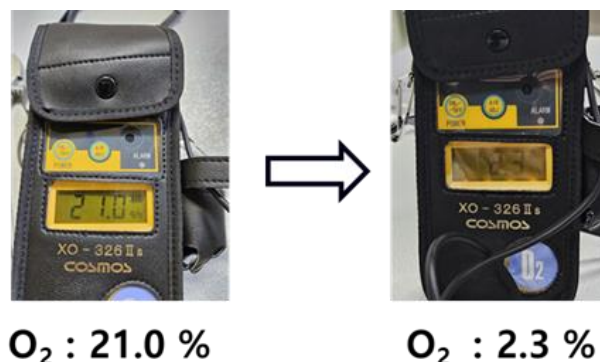

Figure 10.
Maintenance of low-oxygen atmosphere ($O_2 \leq 3\%$).

3.2. Comminution and Electrolyte-Removal Performance

A batch of five spent cylindrical LIB cells (DBK, 18650, Ø18 mm × 65 mm) was processed under the continuous inert-atmosphere protocol. As shown in Figure 11, the pre-shredding mass of the batch was 236.09 g, and the post-shredding collected solids weighed 223.61 g. The corresponding mass loss of 12.48 g is attributed to removal of volatile electrolyte and entrained moisture during the 300 °C drying step. Normalized to the initial mass, this yields an electrolyte-removal fraction of 5.3%, with the remaining 94.7% recovered as solid fragments (current collectors, active materials, casing), in agreement with the mass balance summarized in Table 1. These values are consistent with literature ranges for carbonate-based electrolytes in 18650-class cells and indicate effective solvent removal under the specified dwell. Minor uncertainties arise from residual solvent adsorption and scale readability; nevertheless, mass closure (94.7% + 5.3% ≈ 100%) confirms process consistency.

Figure 11.
Spent cylindrical LIBs before and after treatment. (A) Five 18650 cells prior to shredding (batch mass 236.09 g) (B) Collected shredded solids after inert shredding and 300 °C drying (mass 223.61 g).

Table 1.
Mass balance for five spent 18650 cells before vs. after shredding/drying

Condition	Mass (g)	Share (%)
Pre-shredding (5 cells)	236.09	100
Post-shredding solids	223.61	94.7
Removed electrolyte (by difference)	12.48	5.3

3.3. Metal-Bearing "Black Powder": Size Classification and Phase/Composition Analysis

To characterize the final pre-treatment product ("black powder") for recycling, the shredded solids were dry-sieved into narrow size fractions (Figure 12) and each fraction was weighed to close the mass balance (Table 2). Because the typical cathode/anode fragments and current-collector foils in spent 18650 cells range from tens of micrometers to several millimeters, the sieve stack covered >4.0 mm, 1.0–4.0 mm, 600 µm–1.0 mm, 106 µm–600 µm, 38 µm–106 µm, and <38 µm. The post-classification totals reproduced the bulk mass (223.53 g) within 0.08 g, the small difference being attributed to handling loss during sieving. Most of the mass resided in coarse pieces >4.0 mm (81.54%), consisting largely of casing fragments and folded foils; the next most abundant bins were 1.0–4.0 mm (6.97%) and 106 µm–600 µm (≈6.97%), followed by 600 µm–1.0 mm (2.93%). Fine fractions were minor: 38–106 µm (0.65%) and <38 µm (1.07%). This distribution indicates that, under low-speed/high-torque comminution, the process preferentially liberates large foil pieces while still generating a fine black powder suitable for downstream separation.
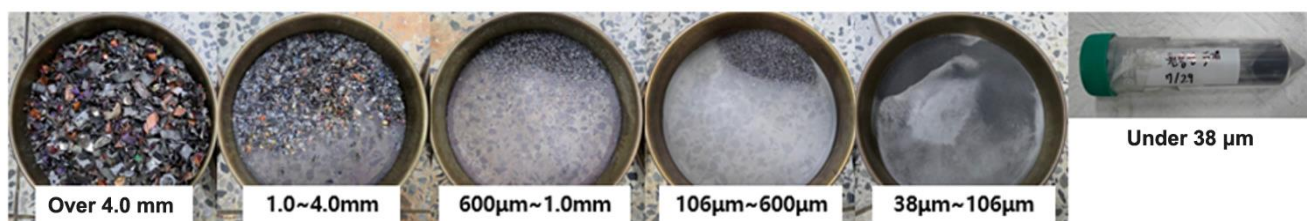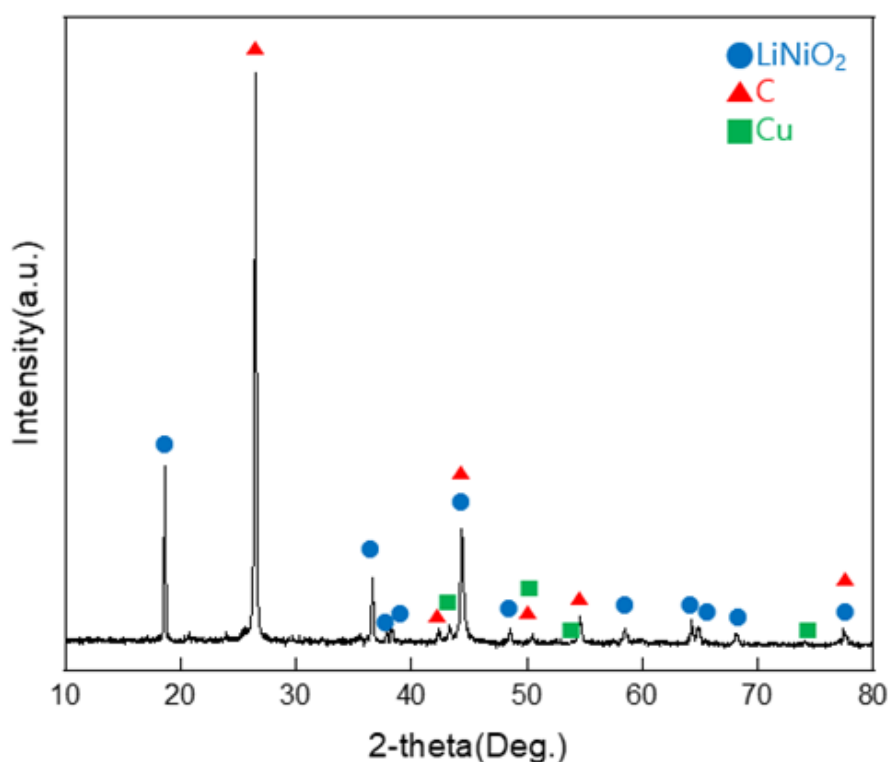

Figure 12.
Size classification by sieving of the shredded product into six fractions from >4.0 mm down to <38 µm.

Table 2.
Mass distribution of the shredded product by size class.

Size class	Mass (g)	Share (%)
> 4.0 mm	182.26	81.54
1.0 – 4.0 mm	15.57	6.97
600 μm – 1.0 mm	6.54	2.93
106 μm – 600 μm	15.57	6.97
38 μm – 106 μm	1.45	0.65
< 38 μm	2.4	1.07
Sum	223.53	100

Phase identification on the <38 μm powder by XRD (Fig. 13) confirmed the presence of $LiNiO_2$–type cathode reflections along with graphitic carbon (C) from the anode and copper (Cu) from the current collector. Other metal phases were comparatively weak or indistinct, likely due to low abundance and partial amorphization during service and comminution. Bulk elemental analysis by XRF yielded a representative transition-metal composition of Ni 28.30 wt%, Co 10.93 wt%, and Mn 14.06 wt%, consistent with an NCM-family cathode for the tested cylindrical cells. These results verify that the product stream contains recoverable metals in forms amenable to established hydrometallurgical or pyrometallurgical recovery routes.

Figure 13.
XRD pattern of the <38 μm "black powder" showing characteristic peaks indexed to $LiNiO_2$ (cathode),
C (graphite, anode), and Cu (current collector), consistent with an NCM-type chemistry indicated by XRF.

Table 3.
XRF composition of the < 38 μm "black powder" fraction recovered from spent cylindrical Li-ion batteries (18650), reporting transition-metal and current-collector elements (wt%)

Element	Ni	Fe	Mn	F	Co	Cu	P	Al	Si	S	Zn	Ca	Cr
Weight (%)	28.30	14.27	14.06	11.75	10.93	9.52	6.51	3.54	0.52	0.20	0.20	0.13	0.07

To examine metal distribution and concentration in the < 38 μm "black-powder" fraction, we performed SEM–EDS mapping and point/area quantification. As shown in Figure 14 and Figure 15, the elemental maps display strong signals of Ni, Mn, and Co—the principal constituents of the NCM-type cathode—indicating that a substantial portion of the active material remains intact after shredding and drying under inert atmosphere. Signals of Cu and Al are also present and are attributed to fragments of the current collectors; weak P features are consistent with phosphate/fluorophosphate residues originating from the electrolyte salt.
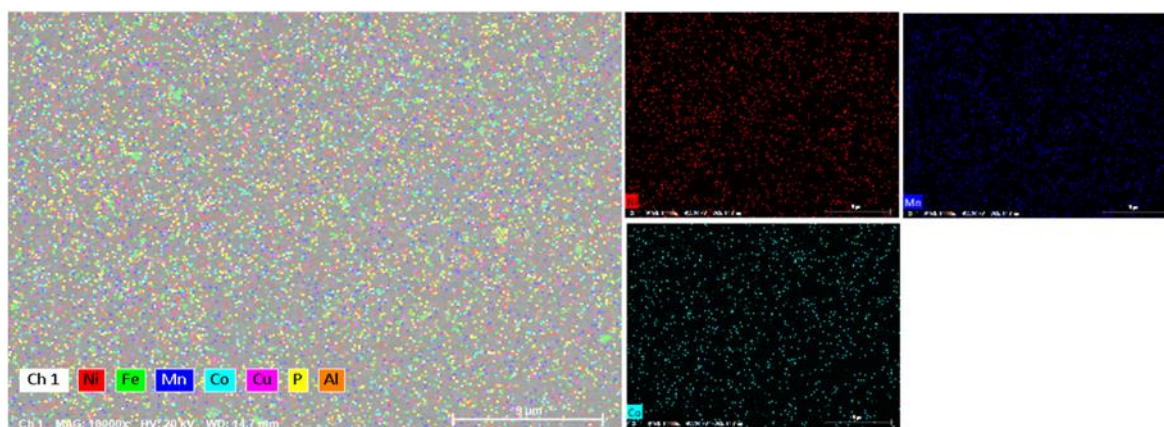
Figure 14.
SEM–EDS elemental maps of the < 38 µm black-powder fraction (≈50×).
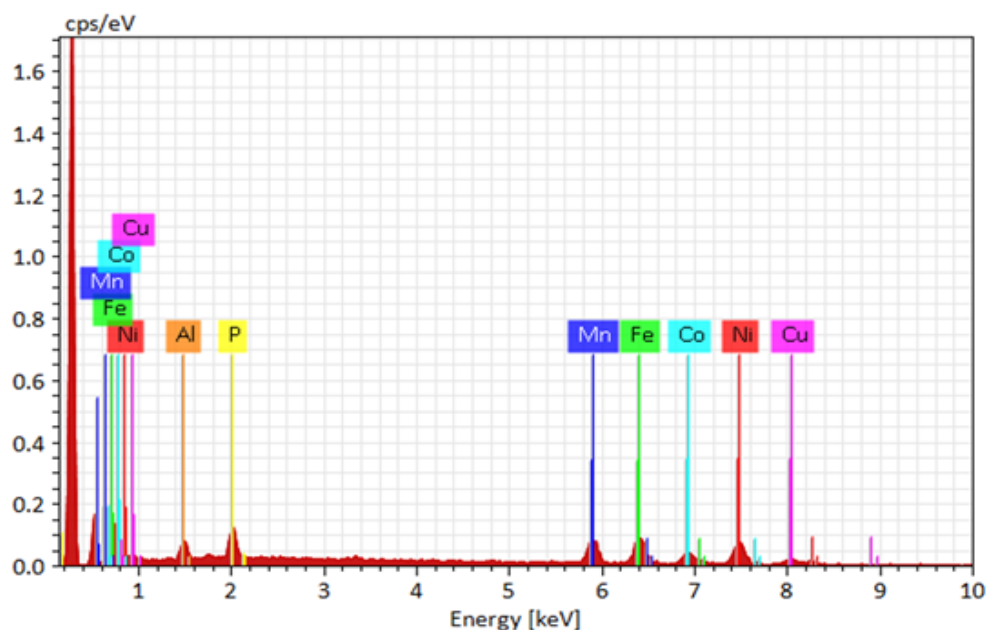

Figure 15.
Representative EDS spectrum from the < 38 µm fraction with peak assignments for Ni, Mn, Co, Cu, Al, Fe, and P

Quantitative results from the mapped area are summarized in Table 4. Using the raw EDS weight percentages, the sum of NCM metals is Ni 10.66 wt% + Mn 6.37 wt% + Co 4.84 wt% = 21.87 wt%. This level is close to literature values for spent NCM cells (e.g., 24.03 ± 0.69 wt% for cathode metals reported previously), supporting the interpretation that the present discharge-free, low-O_2 pre-treatment did not incur appreciable loss of active-material metals. Differences between Table 3 (bulk XRF) and Table 4 (local EDS) are expected: XRF provides a bulk-averaged composition over the entire pressed powder with minimal matrix bias, whereas EDS is surface/locale-specific and sensitive to particle orientation, roughness, and matrix effects; therefore, EDS values reflect local heterogeneity while XRF reflects the ensemble average. Taken together, the mapping and spectra confirm that the black-powder stream retains recoverable Ni–Mn–Co along with Cu/Al from collectors, suitable for downstream hydrometallurgical routes.

Table 4.
Quantitative SEM–EDS results for the < 38 µm black-powder fraction (reported as measured wt% and normalized wt%; atomic % and 1-σ errors also shown)

Element	At.No.	Netto	Mass (%)	Mass Norm. (%)	Atom (%)	abs. error (%) (1 sigma)	Rel.error (%) (1 sigma)
Ni	28	2161	10.66	28.11	24.57	0.65	6.05
Fe	26	2188	7.41	19.54	17.94	0.42	5.65
Mn	25	2180	6.37	16.79	15.67	0.36	5.58
Co	27	1098	4.84	12.75	11.10	0.32	6.69
Cu	29	605	3.79	9.99	8.06	0.31	8.10
P	15	1759	2.68	7.06	11.69	0.17	6.20
Al	13	942	2.19	5.77	10.98	0.19	8.50
Sum			39.93	100.00	100.00		

3.4. Comparison with Conventional Brine-Discharge Pre-Treatment

We benchmarked the developed apparatus against the conventional flow that relies on salt-solution discharge → shredding → drying/washing. The proposed system executes shredding and thermal electrolyte removal entirely under an inert atmosphere without a brine step, while continuously controlling oxygen at ≤ 3% and neutralizing acid off-gases via a wet scrubber. In practice, this eliminates odorous, metal-bearing wastewater; reduces explosion risk associated with residual energy during shredding; and enables continuous, automation-ready operation rather than stop-and-go batch handling. The integrated dryer–scrubber train further shortens cycle time by avoiding post-wash drying.

Table 5.
Comparison between a conventional brine-discharge process and the present apparatus

Aspect	Conventional (Brine discharge–based)	This work (Inert, discharge-free apparatus)
Discharge method	Brine immersion (wastewater, odor generation)	Not required; inert (Ar) atmosphere maintained
Shredding safety	Risk of spark/explosion if discharge incomplete	O_2 controlled to ≤ 3% during shredding
Electrolyte removal	Requires drying and often washing	In-chamber drying in inert gas; no washing
Off-gas handling	Often vented/oxidized; limited neutralization	Wet scrubber with NaOH/BTB for HF/HCl neutralization
Process mode	Batch, frequent stops and operator intervention	Continuous feed via pass-box; automation-ready

4. Conclusions

This study developed and experimentally validated an inert-atmosphere, discharge-free pre-treatment system for spent lithium-ion batteries that enables shredding and thermal drying without spark, fire, or explosion risk. The apparatus integrates a pass-box with an all-in-one processing enclosure (shredder + drying furnace) and maintains the internal oxygen concentration at ≤ 3%, thereby suppressing oxidation of solid electrolyte residues and organic carbonate solvents. Compared with the conventional brine-discharge → shredding → drying route, the proposed design reduces environmental burden (no wastewater or odor), supports continuous operation, and incorporates a wet scrubber that effectively neutralizes HF/HCl evolved during electrolyte removal—features that collectively increase its practicality for industrial deployment.

Performance tests on cylindrical 18650 cells demonstrated robust comminution and solvent removal. The measured electrolyte-removal fraction was 5.3% by mass balance, and the recovered "black powder" exhibited metal contents comparable to those from conventional lines, confirming uniform thermal treatment and effective liberation of active material without composition loss. These outcomes indicate that discharge can be safely omitted when atmosphere control and exhaust neutralization are properly implemented. The present work was conducted at pilot scale; consequently, future studies should assess throughput at industrial scales, energy consumption, and maintenance logistics under continuous operation. Additional tasks include detailed speciation of off-gases during thermal treatment, quantitative analysis of residual electrolyte, and end-to-end evaluation of metal recovery yield from the black-powder stream. In summary, the proposed system offers a viable alternative to brine-based pre-treatment: it is environmentally cleaner, automation-ready, and intrinsically safer. As such, it provides a credible pathway toward adoption as a core unit operation in next-generation, large-scale recycling of spent lithium-ion batteries.

References

[1] Grand View Research, "Lithium-ion battery market size, share & trends analysis report by product, 2025–2033 (Report No. SE 4967)," San Francisco, CA: Grand View Research, 2025.

[2] Statista, *Mobility markets – electric vehicles: Market data analysis & forecast (Worldwide)*. Hamburg, Germany: Statista, 2022.

[3] M. Bhar, S. Ghosh, S. Krishnamurthy, Y. Kaliprasad, and S. K. Martha, "A review on spent lithium-ion battery recycling: From collection to black mass recovery," *RSC Sustainability,* vol. 1, no. 6, pp. 1150–1167, 2023. https://doi.org/10.1039/d3su00086a

[4] J. Neumann *et al.*, "Recycling of lithium-ion batteries—current state of the art, circular economy, and next generation recycling," *Advanced Energy Materials,* vol. 12, no. 21, p. 2102917, 2022. https://doi.org/10.1002/aenm.202102917

[5] V.-M. Omar, J. Valio, A. Santasalo-Aarnio, M. Reuter, and R. Serna-Guerrero, "A critical review of lithium-ion battery recycling processes from a circular economy perspective," *Batteries,* vol. 5, no. 4, p. 68, 2019. https://doi.org/10.3390/batteries5040068

[6] M. Kaya and H. Delavandani, "State-of-the-art lithium-ion battery pretreatment methods for the recovery of critical metals," *Minerals,* vol. 15, no. 5, p. 546, 2025. https://doi.org/10.3390/min15050546

[7] D. Zsolt, T. Dinh, and T. Kulcsár, "A review on recycling of spent lithium-ion batteries," *Energy Reports,* vol. 9, pp. 6362-6395, 2023. https://doi.org/10.1016/j.egyr.2023.05.264

[8]   D. Sturk, L. Rosell, P. Blomqvist, and A. Ahlberg Tidblad, "Analysis of li-ion battery gases vented in an inert atmosphere thermal test chamber," *Batteries,* vol. 5, no. 3, p. 61, 2019. https://doi.org/10.3390/batteries5030061

[9]   K. Gholamreza, K. Javdan Tabar, A. H. Homayouni, and S. Chehreh Chelgani, "Recycling spent lithium batteries – an overview of pretreatment flowsheet development based on metallurgical factors," *Environmental Technology Reviews,* vol. 12, no. 1, p. 2248559, 2023. https://doi.org/10.1080/21622515.2023.2248559

[10]   Tetsuya Uda, Akihiro Kishimoto, Kouji Yasuda, and Yu-ki Taninouchi, "Submerged comminution of lithium-ion batteries in water in inert atmosphere for safe recycling," *Energy Advances,* vol. 1, pp. 935–940, 2022. https://doi.org/10.1039/d2ya00202g